Cyclotron Production and PET/MR Imaging of ^{52}Mn

A. Lake Wooten[a,b], Benjamin C. Lewis[a,c], Richard Laforest[a], Suzanne V. Smith[d], Suzanne E. Lapi[a,b,1]

[a]Mallinckrodt Institute of Radiology, Washington University School of Medicine, St. Louis, MO, United States
[b]Department of Biomedical Engineering, Washington University in St. Louis
[c]Department of Physics, Washington University in St. Louis
[d]Collider-Accelerator Department, Brookhaven National Laboratory, Upton, NY, United States

Introduction

The goal of this work is to advance the production and use of ^{52}Mn ($t_{1/2}$=5.6 d, β^+: 242 keV, 29.6%) as a radioisotope for *in vivo* preclinical nuclear imaging. More specifically, the aims of this study were: (1) to measure the excitation function for the ^{nat}Cr(p,n)^{52}Mn reaction at low energies to verify past results [1-4]; (2) to measure binding constants of Mn(II) to aid the design of a method for isolation of Mn from an irradiated Cr target via ion-exchange chromatography, building upon previously published methods [1,2,5-7]; and (3) to perform phantom imaging by positron emission tomography/magnetic resonance (PET/MR) imaging with ^{52}Mn and non-radioactive Mn(II), since Mn has potential dual-modality benefits that are beginning to be investigated [8].

Material and Methods

Thin foils of Cr metal are not available commercially, so we fabricated these in a manner similar to that reported by Tanaka and Furukawa [9]. ^{nat}Cr was electroplated onto Cu discs in an industrial-scale electroplating bath, and then the Cu backing was digested by nitric acid (HNO_3). The remaining thin Cr discs (~1 cm diameter) were weighed to determine their thickness (~75-85 µm) and arranged into stacked foil targets, along with ~25 µm thick Cu monitor foils. These targets were bombarded with ~15 MeV protons for 1-2 min. at ~1-2 µA from a CS-15 cyclotron (The Cyclotron Corporation, Berkeley, CA, USA). The beamline was perpendicular to the foils, which were held in a machined 6061-T6 aluminum alloy target holder. The target holder was mounted in a solid target station with front cooling by a jet of He gas and rear cooling by circulating chilled water (T≈2-5 °C). Following bombardment, these targets were disassembled and the radioisotope products in each foil were counted using a high-purity Ge (HPGe) detector. Cross-sections were calculated for the ^{nat}Cr(p,n)^{52}Mn reaction.

Binding constants of Mn(II) were measured by incubating ^{54}Mn(II) ($t_{1/2}$=312 d) dichloride with anion- or cation-exchange resin (AG 1-X8 (Cl^- form) or AG 50W-X8 (H^+ form), respectively; both: 200-400 mesh; Bio-Rad, Hercules, CA) in hydrochloric acid (HCl) ranging from 10 mM-8 M (anion-exchange) and from 1 mM-1 M (cation-exchange) or in sulfuric acid (H_2SO_4) ranging from 10 mM-8 M on cation-exchange resin only. The amount of unbound ^{54}Mn(II) was measured using a gamma counter, and binding constants (K_D) were calculated for the various concentrations on both types of ion-exchange resin.

We have used the unseparated product for preliminary PET and PET/MR imaging. ^{nat}Cr metal was bombarded and then digested in HCl, resulting in a solution of Cr(III)Cl_3 and ^{52}Mn(II)Cl_2. This solution was diluted and imaged in a glass scintillation vial using a microPET (Siemens, Munich, Germany) small animal PET scanner. The signal was corrected for abundant cascade gamma-radiation from ^{52}Mn that could cause random false coincidence events to be detected, and then the image was reconstructed by filtered back-projection. Additionally, we have used the digested target to spike non-radioactive Mn(II)Cl_2 solutions for simultaneous PET/MR phantom imaging using a Biograph mMR (Siemens) clinical scanner. The phantom consisted of a 4x4 matrix of 15 mL conical tubes containing 10 mL each of 0, 0.5, 1.0, and 2.0 mM concentrations of non-radioactive Mn(II)Cl_2 with 0, 8, 17, and 33 µCi (corrected to start of PET acquisition) of ^{52}Mn(II)Cl_2 from the digested target added. The concentrations were based on previous MR studies that measured spin-lattice relaxation time (T1) versus concentration of Mn(II), and the activities were based on calculations for predicted count rate in the scanner. The PET/MR imaging consisted of a series of two-dimensional inversion-recovery turbo spin echo (2D-IR-TSE) MR sequences (TE=12 ms; TR=3,000 ms) with a wide range of inversion times (TI) from 23-2,930 ms with real-component acquisition, as well as a 30 min. list-mode PET acquisition that was reconstructed as one static frame by 3-D ordered subset expectation maximization (3D-OSEM). Attenuation correction was performed based on a two-point Dixon (2PD) MR sequence. The DICOM image files were loaded, co-registered, and windowed using the Inveon Research Workplace software (Siemens).

[1]Corresponding author, E-mail: lapis@mir.wustl.edu

Results and Conclusion

Cross-sections were measured for the $^{nat}Cr(p,n)^{52}Mn$ reaction. The highest cross-section measured was σ=0.15 b, which occurred at the highest energy measured of E_p=14.0 MeV. This is in agreement with previous work [1,4].

In the binding studies, $^{54}Mn(II)$ bound quite effectively (K_D>10^3 mL/g) to the cation-exchange resin at low concentrations of HCl (1, 10, 50 mM), but its binding then decreased with higher concentration, reaching K_D=1.2 mL/g at 3 M HCl. Similarly, the binding of $^{54}Mn(II)$ to a cation-exchange resin in H_2SO_4 was also high (K_D>10^2) at lower acid concentrations (10 and 100 mM) and decreased with increasing H_2SO_4, reaching no measured binding at 3 and 8 M. With the anion-exchange resin, a slight trend suggested $^{54}Mn(II)$ bound more effectively to the anion-exchange resin with increasing HCl, but the maximum value of K_D=1.7 mL/g at 8 M HCl was very small. Additionally, we found that the presence of ethanol in HCl solutions significantly affected the binding of $^{54}Mn(II)$ with either resin.

Phantom PET and PET/MR imaging were performed, with the idea that non-radioactive Mn(II) would provide T1-shortening contrast in T1-weighted MRI and the ^{52}Mn would provide PET signal. Figure 1 shows clearly the increased counts from PET as the activity of ^{52}Mn added increased from top to bottom. It also shows decreasing MR signal as the concentration of cold Mn(II) increased from left to right. This occurs because TI (2,930 ms) for the MR in Figure 1 was long enough for the solutions with longer T1 (less Mn(II)) to relax to a more positive magnetization (brighter signal) compared to vials containing more Mn(II), shown in shades of gray that still show positive signal (gray=zero; black=negative). However, we also noticed that the MR signal decreases from top to bottom. We believe that this change in MR signal was not from the added ^{52}Mn because its highest concentration in any vial was <2 nM, which would be difficult to detect by MRI. Based on the masses of the target foils, we estimate that the concentrations of Cr(III) from the dissolved target was many times the total concentration Mn(II): 0, 8, 16, and 33 mM. It appears that even though Cr(III) has a magnetic moment ~35% less than Mn(II), these high concentrations of Cr(III) have produced significant T1 shortening signal in the MR imaging. This MR artifact from Cr(III) supports the importance for effective separation of ^{52}Mn. Future imaging of separated ^{52}Mn product should have minimal effect on MR signals.

In summary, we have produced thin ^{nat}Cr discs that were bombarded in stacked foil experiments to measure cross-sections and to produce ^{52}Mn for PET/MR imaging in a clinical scanner. We have also performed ion-exchange binding experiments that will support ongoing work on separating ^{52}Mn from a Cr target. Finally, we have conducted preliminary imaging studies investigating ^{52}Mn as a PET agent that could be a tool for studying contrast agents for manganese-enhanced MRI (MEMRI).

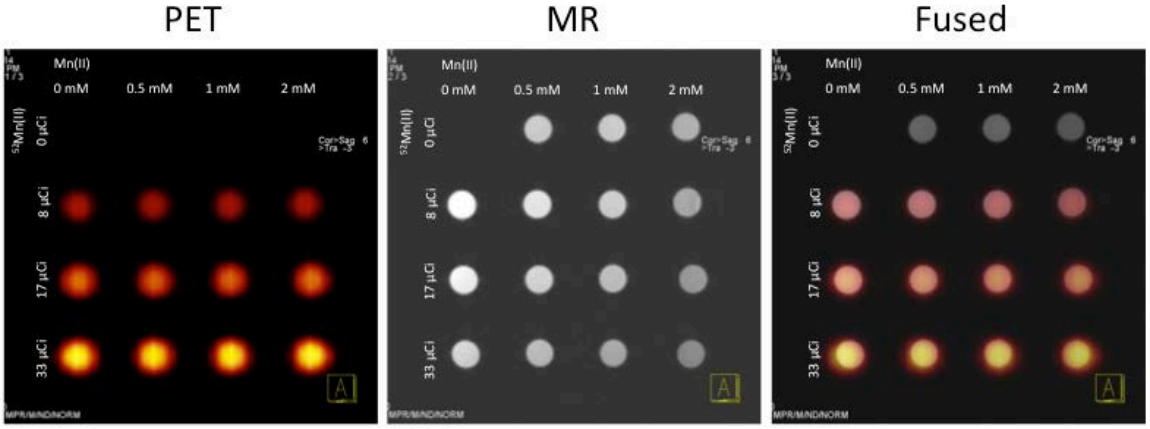

FIGURE 1. PET/MR images of a phantom consisting of vials containing non-radioactive Mn(II) and unseparated $^{52}Mn(II)$ (with Cr(III)). PET: A 30 min. list-mode PET acquisition that was reconstructed as one static frame. Attenuation correction was performed by two-point Dixon sequence. (Radioactivity labels were corrected to the start of PET data acquisition.) MR: A two-dimensional inversion-recovery turbo spin echo MR sequence (TE=12 ms; TR=3,000 ms; TI 2,930 ms) with real-component acquisition.

References

1. M. Buchholz, I. Spahn, B. Scholten, H.H. Coenen: *Radiochim. Acta*, **101**, pp. 491-499, 2013.
2. A.T.J. Klein, F. Rosch, S.M. Qaim: *Radiochim. Acta*, **88**, pp. 253-264, 2000.
3. J.R. Walton, D. Heymann, A. Yaniv, D. Edgerley, M.W. Rowe: *J. Geophys. Res.*, **81**, pp. 5689-5699, 1976.
4. J.N. Barrandon, J.L. Debrun, A. Kohn, R.H. Spear: *Nucl. Instr. Meth.* **127**, pp. 269-278, 1975.
5. G.J. Topping, P. Schaffer, C. Hoehr, T.J. Ruth, V. Sossi: *Med. Phys.*, **40**, pp. 042502, 2013.
6. S. Lahiri, D. Nayak, G. Korschinek: *Anal. Chem*, **78**, pp. 7517-7521, 2006.
7. A.T.J. Klein, F. Rosch, H.H. Coenen, S.M. Qaim: *Radiochim. Acta*, **90**, pp. 167-177, 2002.
8. A.T.J. Klein, F. Rosch, H.H. Coenen, S.M. Qaim: *Appl. Radiat. Isot.*, **62**, pp. 711-720, 2005.
9. S. Tanaka, M. Furukawa: *J. Phys. Soc. Japan*, **14**, pp. 1269-1275, 1959.

Acknowledgements

The authors are grateful for valuable contributions from the following core facilities at WUSM: the Cyclotron Facility, the Instrument Machine Shop, the Electronics Shop, the Small Animal Imaging Core, and the Center for Clinical Imaging Research, as well as from a local business, Four Star Finishing (St. Louis). We also appreciate helpful advice from Tara E. Mastren and Xingyu Nie, both from the Lapi group.

This work was funded in part by the National Nuclear Security Administration, U.S. Department of Energy (DE-NA0000979), and A.L.W. was funded in part by a training grant from the U.S. National Institutes of Health (1T32EB14855-01).